The Clay Minerals Society Workshop Lectures Series, Vol. 21 (2016), Chapter 15, 199–210

HYDRATION OF FEBEX BENTONITE AS OBSERVED BY ENVIRONMENTAL SCANNING ELECTRON MICROSCOPY (ESEM)

Frank Friedrich[1,*], Dieter Schild[1],
Peter G. Weidler[2], and Thorsten Schäfer[1]

[1]*Karlsruhe Institute of Technology, Institute for Nuclear Waste Disposal (INE), Hermann-von-Helmholtz-Platz 1, D-76344 Eggenstein-Leopoldshafen, Germany*
[2]*Karlsruhe Institute of Technology, Institute for Functional Interfaces (IFG), Hermann-von-Helmholtz-Platz 1, D-76344 Eggenstein-Leopoldshafen, Germany*
[*]*e-mail: fwfriedrich@googlemail.com*

An environmental scanning electron microscope was used to study the sorption of water by Febex bentonite as a function of relative humidity (RH). The hydration isotherms measured had an exponential shape with strong swelling of the clay particles occurring at high RH (>85%) in particular. The two branches of the isotherm did not overlap and a hysteresis of type H3 was observed which, in gas-adsorption studies, is typical of plate-like particles with slit-shaped pores. Hydration experiments with cation-exchanged bentonite samples revealed that the influence of the interlayer cations on the hydration behavior and swelling of the bentonite was not as pronounced as suspected. In fact, the Sr form showed significantly greater swelling at low RH but the swelling behavior of Li- or Na-exchanged and untreated bentonite samples with mixed interlayer cations was very similar over the entire range of RH. The observed hysteresis for water adsorption and desorption isotherms might thus be attributed both to structural factors, such as changes in pore size and pore geometry, and to the effects of the interlayer cations (*e.g.* varying hydration forces).

1. Introduction

One important application of bentonites is their use in geo-engineered barriers in the context of deep geological repositories for high-level (nuclear) waste (HLW) (*e.g.* Fernández *et al.,* 2004). In the concept for HLW repositories in crystalline formations, the canisters are emplaced in horizontal or vertical drifts and surrounded by a compacted bentonite barrier. The safety concept is built on multiple barriers (engineered, geo-engineered, and geologic) and the stability of the bentonite barrier against erosion by low-mineralized groundwater is a key aspect of the usual evolution scenario. Bentonites with various compositions have been discussed as suitable materials for the geo-engineered barrier. Because of their interlayer chemistry, the swelling behavior of bentonites is an important aspect. The interlayer chemistry is triggered by the water adsorption of smectites, a complex process related to their structural and physical-chemical properties (Bergaya and Lagaly, 2006). The structure of smectites is characterized by

DOI: 10.1346/CMS-WLS-21.15

isomorphous ion replacements which cause a deficit of positive charge in their octahedral and sometimes tetrahedral sheets. This deficit is balanced by interlayer cations such as Na^+ and K^+ or Mg^{2+} and Ca^{2+}. In an aqueous environment in smectites these cations are accessible to water molecules. The water molecules are arranged in a partly ordered structure forming one or two water layers around the interlayer cations, leading to an increased interlayer space. The interlayer cations play an important role, therefore, in the interaction between smectite and water. Not only does the interlayer spacing of the clay mineral depend on the kind of cation, but also on the amount of water adsorbed, thus leading to a strongly increased particle volume and resulting, finally, in a complete delamination of the aggregates, forming colloidal suspensions or voluminous clay gels (Lagaly *et al.,* 1997).

Environmental scanning electron microscopy (ESEM) offers a unique opportunity to investigate sensitive and even wet materials (*e.g.* Donald, 1998; Kloprogge *et al.,* 2005; Stokes, 2008). Due to its ability to adjust the RH around the sample very precisely, ESEM is an excellent tool for the investigation of the swelling behavior of clays (*e.g.* Becker and Dohrmann, 2000; Montes-H *et al.,* 2003a; Carrier *et al.,* 2013). The emphasis for the current study was, therefore, placed on the *in situ* electron microscopic quantification of the swelling of different cation-exchanged bentonite samples, which was then compared with that of the raw material.

2. Materials and methods

2.1. Material

In the present study the Spanish Febex bentonite from Almeria was used. According to Fernandez *et al.* (2004), this raw bentonite is very rich in montmorillonitic clay minerals (>90%), with minor amounts of quartz, feldspars, and cristobalite. For the hydration experiments the <2 μm fraction of untreated bentonite with its natural exchangeable cation population was used. This sample is referred to below as 'untreated bentonite.' Twenty g of the clay was purified in accordance with the procedure established by Tributh and Lagaly (1986).

X-ray diffraction (XRD) and Fourier transform infrared spectroscopy of this fraction revealed only traces of quartz. The clay consisted of an interstratified illite-montmorillonite mineral with 13% of non-swellable layers (data not shown), in good agreement with Cuadros and Linares (1996).

According to the procedure of Glaus *et al.* (2007), Li-, Na-, and Sr-exchanged samples were produced by adding 250 mL of 1 M metal chloride solutions to 2 g of the bentonite <2 μm fraction and shaking the suspensions for 24 h. The clay was then separated by centrifugation (10 min at 1400x*g*) and decantation of the supernatant solutions. The procedure was repeated three times. To remove excess salts, the suspensions were dialyzed in dialysis tubes (Nadir, pore size = 2.5 nm) which had previously been boiled in water to remove soluble organics. The tubes filled with cation-saturated samples were placed in deionized water that was refreshed continually until its electrical

conductivity was <5 μS/cm. All clay samples were then dried at 60°C for 72 h and then ground. To achieve a smectite with reduced layer charge, 2 g of the Li-exchanged sample was heated to 300°C. At this temperature the Li^+ cations migrated from the interlayer space into the mineral framework of the smectite and reduced its layer charge remarkably (Hofmann and Klemen, 1950).

2.2. Environmental scanning electron microscopy (ESEM)

All microscopic measurements were carried out in an FEI Quanta 650 field emission gun environmental scanning electron microscope (FEG-ESEM), which was equipped with a gaseous secondary electron detector (GSED). The microscope was operated at 20 kV in wet mode under varying water-vapor pressures between 130 and 870 Pa and at a fixed working distance of 9.5 mm. To control the sample temperature during the hydration experiments a water-cooled Peltier cooling stage was used.

Using this instrumentation a defined RH can be created around the specimen by varying water-vapor pressure in the microscope chamber and the temperature of the Peltier stage (= specimen temperature). For example, if the temperature were set to 5°C and water-vapor pressure to 499 Pa, according to the phase diagram of water, a RH of 55% resulted around the specimen (Figure 1).

For isotherm measurements, small amounts of clay powder were poured onto the stainless steel sample holder and the stage temperature and the chamber pressure were set to 5°C and 130 Pa, respectively. According to these parameters the RH around the sample was 15%. The specimen was allowed to equilibrate under these conditions for at least 15 min prior to the start of the experiments.

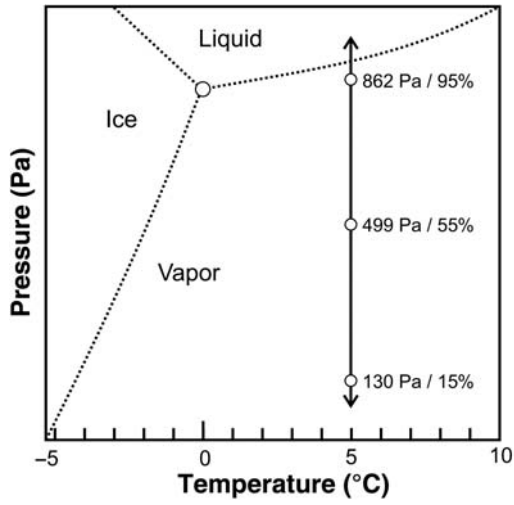

Figure 1. Sketch of the phase diagram of water and the hydration path used for isotherm measurements at 5°C in the ESEM.

To estimate the time to reach equilibrium hydration conditions, the chamber pressure was set at 862 Pa at a fixed temperature of 5°C (95% RH). After 120 s the 'live image' was stable enough and images then were taken every 60 s for a period of 20 min. The chamber pressure was then set back to 130 Pa (15% RH) and again images were taken every 60 s for a period of 20 min.

Swelling isotherms were measured by increasing the water-vapor pressure in five steps from 130 to 862 Pa, which corresponded to values of 15, 35, 55, 75, 85, and 95% RH, respectively. At each pressure step an image was taken after an equilibration time of 15 min. The last step of the hydration cycle at 862 Pa (95% RH) was used as the first step of the dehydration cycle. The chamber pressure was then decreased using the same five steps as in the hydration cycle until the starting conditions were achieved (130 Pa, 15% RH). The sample temperature was always kept constant at 5°C.

For digital image analysis the open source software, *ImageJ*, was used (Rasband, 2015). Bentonite aggregates with diameters between 30 and 50 μm were selected for area measurements. The selected ESEM images were converted to 8-bit and covered areas of 1024 pixels × 943 pixels. The area of interest (AOI) was isolated by applying a gray-level threshold (Figure 2). *ImageJ* considered a gray-level range of 0–255 for all area measurements. The increase in area was then calculated from the following equation:

$$\text{Swelling } (\%) = ((A_h - A_0)/A_0) \times 100 \quad (1)$$

where A_h represents the area (μm^2) of the hydrated sample and A_0 represents the initial area (μm^2) of the dry sample at 5°C and 15% RH. The data were displayed as areal expansion (swelling %) *vs.* RH at a fixed temperature and therefore can be indicated as isotherms.

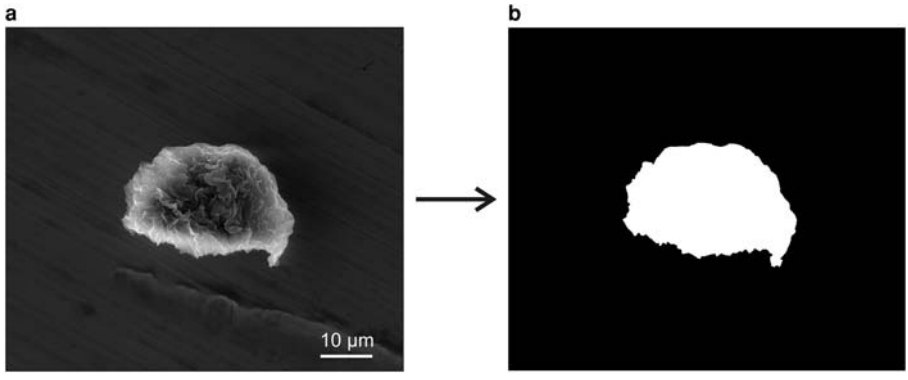

Figure 2. Digital image analysis of the clay: (a) ESEM image; (b) binary image of the selected aggregate, obtained from the image analysis done using *ImageJ* software.

Scanning electron microscopy provides 2D images of three-dimensional particles, which means that only a projection of the clay aggregate surface on the *xy* plane is measurable. Information along the *z* direction is not available. To investigate the behavior of the Febex bentonite along the *z* axis during hydration, a thin clay film with oriented clay platelets was produced by sedimentation from a suspension of the Na-exchanged material with a clay concentration of 5 g/L. A small piece of freshly broken film was then glued vertically to the stainless steel sample holder using a conductive adhesive (Leitsilber, Plano GmbH, Germany). The edge of the clay film was observable directly during later hydration in the ESEM (Figure 3a).

The swelling behavior of the film along the *c* axis of the oriented clay-mineral particles is compared to swelling along their *ab* planes in Figure 3b. The clay particles show a very anisotropic swelling behavior. While the clay film swelled strongly in a direction perpendicular to the clay layers (along the *c* axis); swelling along the *ab* plane occurred only at large RH values (>75%) and to a very small extent. Such behavior was attributed by Carrier *et al.* (2013) to irregularities and misalignments in the particle orientation.

Put simply, in clay aggregates the particles are randomly oriented. According to the results shown in Figure 3b, an equidimensional swelling of these aggregates during a hydration experiment in the ESEM can be assumed. The measured area data display a 2D projection of the volumetric expansion, therefore, and can be used for quantification of the observed clay swelling without further transformation into a coefficient of volume expansion. Similar approaches were used by a number of earlier studies (*e.g.* Montes-H *et al.,* 2003a; Montes-H, 2005; Romero and Simms, 2008; Carrier *et al.*, 2013).

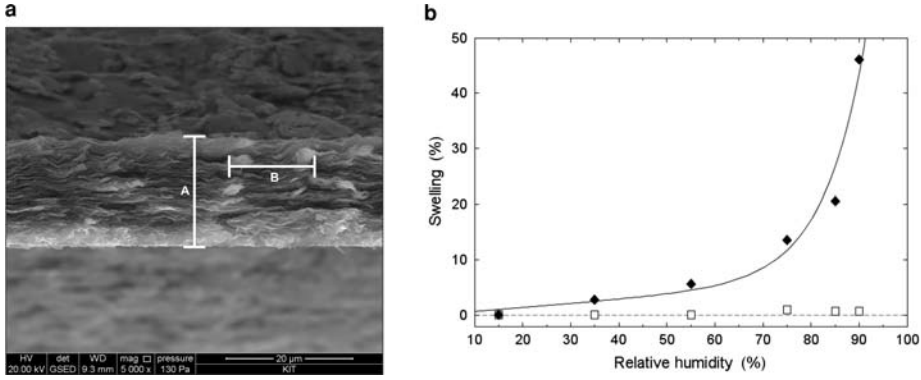

Figure 3. (a) ESEM image of self-supporting Na-Febex film. The bars show the measurement directions: (A) along the *c* axis of the oriented clay particles, (B) perpendicular to the *c* axis of the oriented clay particles. (b) Swelling isotherm measurements of the oriented clay film (Na-Febex). Comparison of the strongly anisotropic swelling behavior parallel and perpendicular to the clay-mineral *c* axis (black diamonds: swelling parallel to *c* axis, white squares: swelling perpendicular to *c* axis).

Table 1. Calculated mean deviation (%) of the swelling percentages of five Na-Febex samples.

RH	Sample 1	Sample 2	Sample 3	Sample 4	Sample 5	Mean swelling ± standard deviation
15	0	0	0	0	0	0
35	1.2	0.5	2.5	2.6	0.9	1.5 ± 1.0
55	3.4	1.6	3.0	4.0	2.5	2.9 ± 0.9
75	5.6	2.9	5.2	6.7	4.3	4.9 ± 1.4
85	9.3	6.4	8.1	9.7	7.9	8.3 ± 1.4
95	36.3	31.2	30.0	34.0	33.8	32.5 ± 2.5

To determine the precision of the hydration experiments, the average standard deviation (SD) was calculated for each hydration step after the measurement of hydration isotherms of five different particles. Representative of the behavior of all bentonite samples, the mean deviation for the Na-exchanged sample is displayed in Table 1. Note that the SD was constant between 0.9 and 1.4% for RH values of up to 85%. Only at the largest RH values did the SD increase slightly to 2.5%. This increase in deviation was probably related to varying amounts of non-swelling domains in the aggregates which should have a greater effect on the aggregate swelling with increasing relative humidities.

3. Results and discussion

The ESEM images of bentonite aggregates during hydration (Figure 4) revealed that the aggregate size increased notably with increasing humidity, and the typical rough smectite morphology also changed considerably. An overlay image of the isolated areas of interest illustrates the swelling process.

Based on XRD investigations of water-vapor adsorption-desorption experiments, many authors have reported a stepwise increase in interlayer spacing and were able to calculate discrete hydration states with one or more water layers (1W, 2W) in smectite interlayers during hydration (*e.g.* Cases *et al.,* 1997; Ferrage *et al.,* 2005, 2007; Emmerich *et al.,* 2015).

This behavior of smectites cannot be observed in microscopic swelling *vs*. RH hydration experiments, however. Only Montes-H *et al.* (2003a) found three hydration states during an experiment with RH levels fixed at 90% or 95%. A similar setup was tested (by the present authors) using a Na-exchanged Febex sample: the RH was first increased from 15 to 90% in one step and held there for 12 min (equilibration time) and then increased further to 97% and held for a further 5 min. The swelling behavior of the aggregate *vs*. time is shown in Figure 5a (black squares). The initial swelling was very quick. As explained above, this process could not be captured in image form. A plateau at 18% swelling was reached after just 2 min. No further increase in swelling was detected thereafter until the RH was increased to 97%. Again, this caused a fast and very notable increase in aggregate swelling up to 52%. At that latest stage, water droplets were visible on the aggregate surfaces.

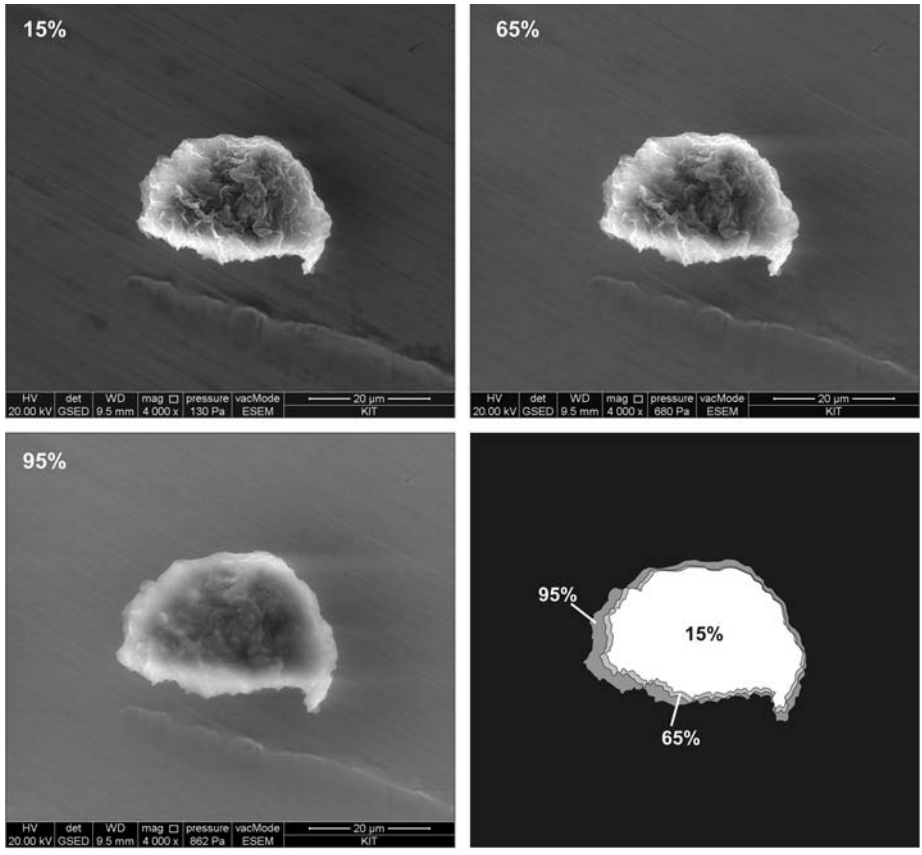

Figure 4. ESEM observation of Febex bentonite aggregates at relative humidities of 15, 65, and 95%, showing remarkable changes in morphology. The overlain assemblage of binary images illustrates the swelling process.

To estimate if these data reflected the occurrence of 1W-layer and 2W-layer states within the sample, two equations developed by Ferrage *et al.* (2005) were used:

$$\text{Layer thickness (1W)} = 12.556 + 0.3525 \times (v/r - 0.241) \times (v \times \text{RH} - 0.979) \quad (2)$$

$$\text{Layer thickness (2W)} = 15.592 + 0.6472 \times (v/r - 0.839) \times (v \times \text{RH} - 1.412) \quad (3)$$

where v is the cation valence, r is the ionic radius, and RH is the relative humidity. For Na^+, $v = 1$ and $r = 0.102$ nm. Equation 2 thus gives a layer thickness of 1.253 nm at 90% RH and with equation 3, a layer thickness of 1.553 nm at 97% RH was calculated. A layer thickness of 1 nm in the dry state (0W) for smectites was also calculated by

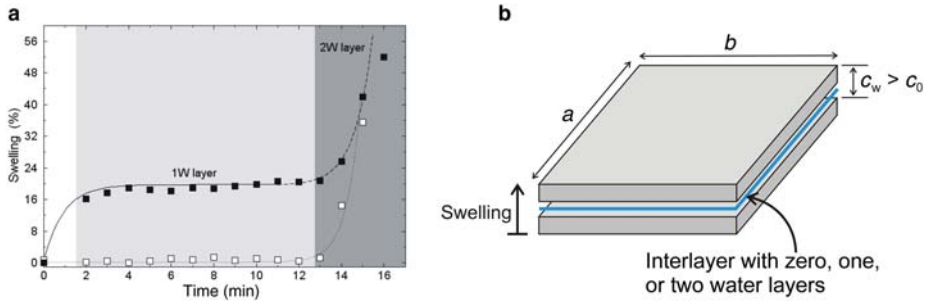

Figure 5. (a) Swelling-shrinkage cycle of Na-Febex at 90% (and after 12 min at 97% RH) to determine equilibration time and occurrence of discrete water layers (1W, 2W) within the smectite interlayer. Filled squares: hydration cycle; open squares: dehydration cycle. Experimental data fitted by exponential functions. (b) Simplified smectite particle used to calculate maximum swelling. C_0: layer thickness without water layer, C_w: layer thickness with one or two water layers incorporated in the interlayer space of smectite.

Ferrage *et al.* (2005). Strictly speaking, the smectite equations of Ferrage *et al.* (2005) cannot be used for an illite-montmorillonite interstratified mineral (*i.e.* the Febex bentonite used in this study), but to demonstrate the general correctness of the assumptions made here a simplified model smectite particle was used. The correct values should be somewhat smaller than the values calculated here.

A sketch of the simplified smectite particle with assumed typical dimensions of 350 nm (*a*), 200 nm (*b*), and the layer thickness values calculated above for 0W, 1W, and 2W (*c*) is shown in Figure 5b. As demonstrated in Figure 3, swelling occurs only along the *c* axis. By comparing the sizes of the *ac* or *bc* planes before and after hydration, therefore, the swelling percentage can be calculated easily. Using the assumed dimensions and layer thicknesses, an area increase of 16% for one water layer (1W) and an increase of 32% for two water layers (2W) can be estimated. These values are in good agreement with the measured data in Figure 5a (18% and 42% swelling). The greater swelling of up to 50% at very high RH values might be explained by a strong contribution of so-called osmotic swelling in the interparticle space as proposed by Baker *et al.* (1995) and Salles *et al.* (2008).

To investigate the dehydration cycle, the first RH value was set at 90% and held for 10 min (equilibration time). To start the dehydration cycle, the RH then was set at 15%. The aggregate immediately lost most of the adsorbed water and shrank to very small swelling percentages (2% after 2 min). The starting size was finally reached after 10 min (open squares). Such timings suggest that 15 min was a sufficient period in which to achieve equilibrium conditions and, thus, this cycle was used for the water-adsorption isotherm measurements.

The water-adsorption isotherm of Na-Febex at 5°C (Figure 6a) revealed that the swelling rates were very small at the beginning of the experiment. Changes in particle morphology did not become clearly visible until RH values of 55%. The swelling increased exponentially at RH values of >75%. The dehydration path proceeded at slightly higher swelling percentages with decreasing RH values. In gas adsorption

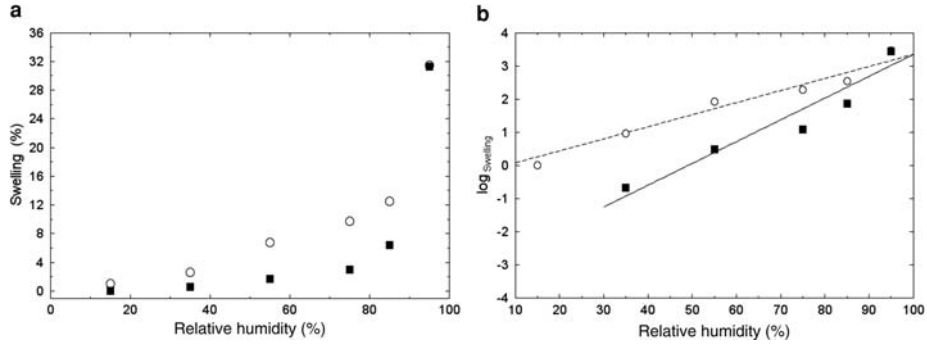

Figure 6. (a) Measured isotherms of Na-Febex bentonite at 5°C. Filled squares: hydration path; open circles: dehydration path. (b) Semi-logarithmic plot of swelling *vs*. relative humidity representing a first-order reaction of the hydration process with hindered dehydration ($t_{equil} = 15$ min).

(BET-) measurements of smectites, similar types of hysteresis were observed. In those cases, this kind of hysteresis loop was referred to as "type H3," and is typical of plate-like particles giving rise to slit-shaped pores (*e.g.* Sing *et al.,* 1985).

A semi logarithmic plot of the swelling data (Figure 6b) yielded a linear function with a slope of 0.061 ± 0.01 ($R^2 = 0.914$) for the hydration path, which is greater than the slope of 0.036 ± 0.004 ($R^2 = 0.967$) for the dehydration path. The hydration exhibits a more pronounced dependence on the RH value than on the reverse action. Similar behavior was observed by several authors using different techniques (*e.g.* Keren and Shainberg, 1975; Fu *et al.,* 1990; Cases *et al.,* 1992) but the interpretation is still the subject of some discussion. From XRD data, the hindered desorption was attributed to decreased entropy (Fu *et al.,* 1990) or to geometrical factors such as changes in particle arrangement and interlayer distances (Cases *et al.,* 1992). In addition, network effects and cavitation phenomena for wide hysteresis loops in mesoporous materials were suggested by Tompsett *et al.* (2005), based on Monte Carlo simulations.

Hydration experiments with various cation-exchanged bentonite samples (Figure 7) yielded fewer differences, as reported in previous studies (*e.g.* Keren and Shainberg, 1975). Untreated, Na- and Sr-exchanged samples swell to a similar maximum (max. = 29 and 28%, respectively), while the swelling of Li-exchanged bentonite was slightly smaller (max. = 18%). Apart from that, the shapes of the hydration paths are very similar for all exchanged cations. In the reduced-layer charge Li sample (Li300) the migration of water molecules into the interlayer was hindered and, thus, swelled to only 6%. Such behavior may have two causes: firstly, the heat treatment leads to the migration of the Li^+ cations into the ditrigonal cavities of tetrahedral sheets, resulting in both a reduction in layer charge and in the amount of interlayer cations. Secondly, the behavior may cause a collapse of the interlayer to an illite-like *d* spacing (*e.g.* Pálková *et al.,* 2003).

The behavior of the untreated sample was similar to that of the Na and Sr samples with a slightly greater maximum swelling (31%), which is related to a mixed

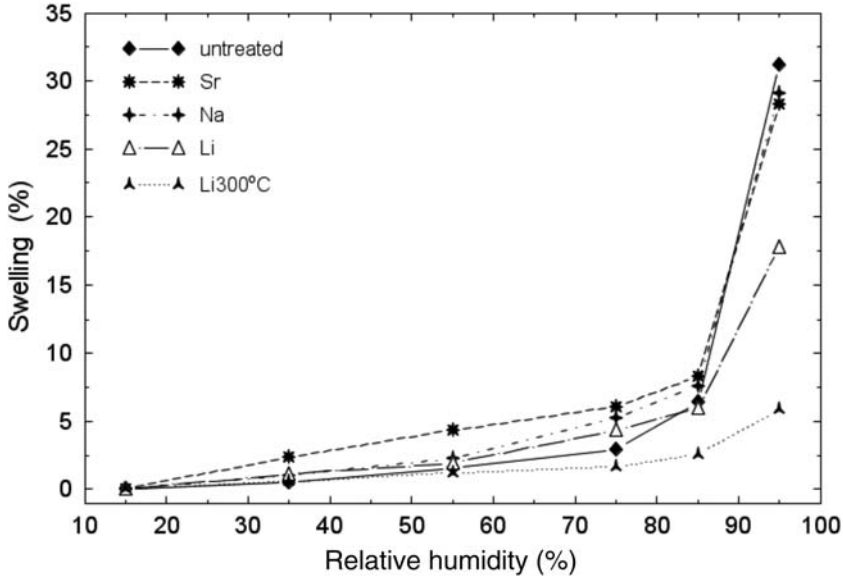

Figure 7. Comparison of the water-adsorption isotherms of Na-, Li-, Li300-, and Sr-exchanged bentonite *vs.* the untreated material.

cation occupancy of its interlayers (Na, Ca). Beyond that, the Sr-saturated bentonite showed significantly greater swelling at low RH values compared to the other samples and this can be assigned to the much greater hydration energy of divalent cations such as Sr ($\Delta H_h^\circ = -1415$ kJ/mol) compared to alkali metals such as Li or Na ($\Delta H_h^\circ = -499$ and -390 kJ/mol) (Wiberg *et al.,* 2007). According to Bol *et al.* (1970), divalent cations form two clear-cut hydration shells which increases the hydration force within the clay interlayers and results in large water spheres around the cations (Keren and Shainberg, 1975). The effect of the kind of interlayer cation on the swelling behavior of the clay aggregates was not as pronounced as discussed by earlier studies, however (*e.g.* Keren and Shainberg, 1975; Montes-H *et al.*, 2003b).

4. Summary and conclusions

Environmental scanning electron microscopy coupled with digital image analysis allowed for *in situ* observation and measurement of the swelling behavior of Febex bentonite in the RH range of 15–95%. New discoveries in terms of the hydration behavior of smectite were not expected from the present study. The behavior of Febex-bentonite in this regard had not been investigated previously, though it has been used in many studies. The hydration behavior of Febex is very significant. Examination of the swelling behavior of Febex, by means of ESEM, showed that it is different from other bentonites, such as MX80, in this regard.

Measurements of the humidity-induced swelling of an oriented Na-exchanged clay film showed a strongly anisotropic swelling behavior with swelling only in the direction perpendicular to the clay stacking. According to these results, and to the simplified assumption of a random distribution of the clay particles in the aggregates, an equidimensional swelling during hydration experiments in the ESEM was a correct assumption.

The hydration isotherms of various cation-exchanged Febex bentonite samples have exponential form with strongly increasing swelling at high RH values. The effect of the kind and charge of interlayer cation seems to be insignificant in this bentonite. The maximum swelling of the Sr, Na, and Li samples is very similar. The hydration paths of the Na, Li, and untreated samples also coincide. Only the Sr-exchanged sample showed significantly more swelling at low RH values, which can be explained by the much greater hydration energy of Sr in comparison with the other ions, and thus its greater hydration force within the clay interlayer.

Acknowledgments

The present work was funded by the Federal Ministry of Economics and Technology (BMWi) under the joint KIT-INE, GRS research project 'KOLLORADO-*e*' (Support code: 02 E 11203B), Germany, and by the European Atomic Energy Community's 7th Framework Program (FP7/2007-2011) under Grant Agreement No. 295487, the BELBaR project.

References

Baker, J.C., Grabowska-Olszewska, B., and Uwins, P.J.R. (1995) ESEM study of osmotic swelling of bentonite from Radzionkow (Poland). *Applied Clay Science*, **9**, 465–469.

Becker, C. and Dohrmann, R. (2000) Environmental Scanning Electron Microscopy (ESEM) – A new method in clay science. *Proceedings of the 6th International Congress on Applied Mineralogy*, ICAM 2000, Göttingen, Germany, 17–19 July 2000, **2**, 719–722.

Bergaya, F. and Lagaly, G. (2006) *Handbook of Clay Science*, 2nd edition. Developments in Clay Science, **5**, Elsevier Science, Amsterdam.

Bol, W., Gerrits, G.J.A., van Panthaleon, and van Eck, C.L. (1970) The hydration of divalent cations in aqueous solution. An X-ray investigation with isomorphous replacement. *Journal of Applied Crystallography,* **3**, 486–492.

Carrier, B., Wang, L., Vandamme, M., Pellenq, R., Bornert, M., Tanguy, A., and Van Damme, H. (2013) ESEM study of the humidity-induced swelling of clay film. *Langmuir*, **29**, 12823–12833.

Cases, J.M., Bérend, I., Besson, G., Francois, M., Uriot, J.P., Thomas, F., and Poirier, J.E. (1992) Mechanism of adsorption and desorption of water vapor by homoionic montmorillonite. 1. The sodium-exchanged form. *Langmuir*, **8**, 2730–2739.

Cuadros, J. and Linares, J. (1996) Experimental kinetic study of the smectite-to-illite transformation. *Geochimica et Cosmochimica Acta*, **60**, 439–453.

Donald, A.M. (1998) Environmental scanning electron microscopy for the study of 'wet' systems. *Current Opinion in Colloid & Interface Science*, **3**, 143–147.

Emmerich, K., Koeniger, F., Kaden, H., and Thissen, P. (2015) Microscopic structure and properties of discrete water layer in Na-exchanged montmorillonite. *Journal of Colloid and Interface Science*, **448**, 24–31.

Fernández, A.M., Baeyens, B., Bradbury, M., and Rivas, P. (2004) Analysis of the porewater chemical composition of a Spanish compacted bentonite used in an engineered barrier. *Physics and Chemistry of the Earth*, **29**, 105–118.

Ferrage, E., Lanson, B., Sakharov, B.A., and Drits, V.A. (2005) Investigation of smectite hydration properties by modeling experimental X-ray diffraction patterns: Part I. Montmorillonite hydration properties. *American Mineralogist,* **90**, 1358–1374.

Ferrage, E., Lanson, B., Sakharov, B.A., Geoffroy, N., Jacquot, E., and Drits, V.A. (2007) Investigation of dioctahedral smectite hydration properties by modeling of X-ray diffraction profiles: Influence of layer charge and charge location. *American Mineralogist*, **92**, 1731–1743.

Fu, M.H., Zhang, Z.Z., and Low, P.F. (1990) Changes in the properties of a montmorillonite-water system during the adsorption and desorption of water: hysteresis. *Clays and Clay Minerals,* **38**, 485–492.

Glaus, M.A., Baeyens, B., Bradbury, M.H., Jakob, A., Van Loon, L.R., and Yaroshchuk, A. (2007) Diffusion of ^{22}Na and ^{85}Sr in montmorillonite: Evidence of interlayer diffusion being the dominant pathway at high compaction. *Environmental Science & Technology*, **41**, 478–485.

Hofmann, U. and Klemen, R. (1950) Verlust der Austauschfähigkeit von Lithiumionen an Bentonit durch Erhitzung. *Zeitschrift für Anorganische Chemie*, **262**, 95–99.

Keren, R. and Shainberg, I. (1975) Water vapor isotherms and heat of immersion of Na/Ca-montmorillonite systems I: homoionic clay. *Clays and Clay Minerals*, **23**, 193–200.

Kloprogge, J.T., Duong, L.V., Frost, R.L., and Boström, T.E. (2005) Use of environmental scanning electron microscopy to study uncoated minerals. *Microscopy and Analysis*, **19**, 17–19.

Lagaly, G., Schulz, O., and Zimehl, R. (1997) *Dispersionen und Emulsionen*. Steinkopff, Darmstadt, Germany.

Montes-H, G. (2005) Swelling–shrinkage measurements of bentonite using coupled environmental scanning electron microscopy and digital image analysis. *Journal of Colloid and Interface Science*, **284**, 271–277.

Montes-H, G., Duplay, J., Martinez, L., and Mendoza, C. (2003a) Swelling/shrinkage kinetics of MX80 bentonite. *Applied Clay Science*, **22**, 279–293.

Montes-H, G., Duplay, J.L., Martinez, L., Geraud, Y., and Rousset-Tournier, B. (2003b) Influence of interlayer cations on the water sorption and swelling-shrinkage of MX80 bentonite. *Applied Clay Science*, **23**, 309–321.

Pálková, H., Madejová, J., and Righi, D. (2003) Acid dissolution of reduced-charge Li- and Ni-montmorillonites. *Clays and Clay Minerals*, **51**, 133–142.

Rasband, W. (2015) *ImageJ* 1.48v. Developed at National Institutes of Health, USA. http://imagej.nih.gov/ij.

Romero, E. and Simms, P.H. (2008) Microstructure investigation in unsaturated soils: A review with special attention to contribution of mercury intrusion porosimetry and environmental scanning electron microscopy. *Geotechnical and Geological Engineering,* **26**, 705–727.

Salles, F., Beurroies, I., Bildstein, O., Jullien, M., Raynal, J., Denoyel, R., and Van Damme, H. (2008) A calorimetric study of mesoscopic swelling and hydration sequence in solid Na-montmorillonite. *Applied Clay Science*, **39**, 186–201.

Sing, K.S.W., Everett, D.H., Haul, R., Moscou, L., Pierotti, R., Rouquerol, J., and Siemieniewska, T. (1985) Reporting physisorption data for gas/solid systems with special reference to the determination of surface area and porosity. *Pure and Applied Chemistry*, **57**, 603–619.

Stokes, D. (2008) *Principles and Practice of Variable Pressure/Environmental Scanning Electron Microscopy (VP-ESEM).* Wiley & Sons, Chichester, UK.

Tompsett, G.A., Krogh, L., Griffin, D.W., and Conner, W.C. (2005) Hysteresis and scanning behavior of mesoporous molecular sieves. *Langmuir*, **21**, 8214–8225.

Tributh, H. and Lagaly, G. (1986) Aufbereitung und Identifizierung von Boden und Lagerstättentonen, I. Aufbereitung der Proben im Labor. *GIT Fachzeitschrift für das Laboratorium*, **30**, 524–529.

Wiberg, N., Wiberg, E., and Holleman, A. (2007) *Hollemann und Wiberg – Lehrbuch der Anorganischen Chemie.* **102**. De Gruyter, Berlin, Germany.